Supplementary

Gunjan Pahlani[1], Thomas Schwartzentruber[1] and Richard D. James[1]†

[1]Department of Aerospace Engineering and Mechanics, University of Minnesota, Minneapolis, MN, 55455, USA

(Received xx; revised xx; accepted xx)

1. Failure of Reiner-Rivlin model

A possible approach to an improved constitutive relation is the Reiner-Rivlin theory (Rivlin 1997; Reiner 1945). That theory assumes the stress to be a function of deformation gradient and the velocity gradient $\boldsymbol{\sigma} = f(\boldsymbol{F}, \nabla \boldsymbol{v})$. When the principle of material frame indifference in addition to the underlying symmetry of the proper unimodular group ($f(\boldsymbol{FU}, \nabla \boldsymbol{v}) = f(\boldsymbol{F}, \nabla \boldsymbol{v})\ \forall \boldsymbol{U},\ \det \boldsymbol{U} = 1$) is used, this dependence reduces to

$$\boldsymbol{\sigma} = \hat{\phi}_0(\rho, I_i(\boldsymbol{d}))\boldsymbol{I} + \hat{\phi}_1(\rho, I_i(\boldsymbol{d}))\boldsymbol{d} + \hat{\phi}_2(\rho, I_i(\boldsymbol{d}))\boldsymbol{d}^2, \tag{1.1}$$

where $\boldsymbol{d} = (\nabla \boldsymbol{v} + \nabla \boldsymbol{v}^T)/2$ and $\hat{\phi}_i$ are coefficients of invariants of tensor $\boldsymbol{d}$ and density of fluid. In contrast to NSF, this model incorporates the non-linearity by taking higher order term of the form $\boldsymbol{d}^2$ but the principle of material frame-indifference implies the collinearity of the stress tensor $\boldsymbol{\sigma}$ and $\boldsymbol{d}$. The Reiner-Rivlin form is investigated by simulating isochoric uniform simple shear flow where $\boldsymbol{A}$ is trace free, rank one tensor of the form $\boldsymbol{A} = \kappa \boldsymbol{e}_1 \otimes \boldsymbol{e}_2$, where flow is in $\boldsymbol{e}_1$ direction, velocity gradient along $\boldsymbol{e}_2$ direction and κ is shear rate. Eigenvectors of $\boldsymbol{d}$ for such flow are uniform in space. Fig. 2(b) compares the evolution of angles $(\theta_{\sigma 1}, \theta_{\sigma 2}, \theta_{\sigma 3})$, $(\theta_{d1} = 45°, \theta_{d2} = 135°, \theta_{d3} = 90°)$ enclosed by $\boldsymbol{e}_1$ direction with the eigenvectors of $\boldsymbol{\sigma}(\sigma 1, \sigma_2, \sigma_3)$, computed from OMD simulations and eigenvectors of $\boldsymbol{d}$ (d_1, d_2, d_3) for simple shear flow. The comparison clearly shows the space independent lagging $(\theta_{\sigma_{1,2}} - \theta_{d_{1,2}} \approx 30°)$ between two tensors $\boldsymbol{\sigma}$ and $\boldsymbol{d}$ which is in contrast to the Reiner-Rivlin and Navier-Stokes theories.

This inadequacy is also supported by the evolution of the molecular density function $f(t, \boldsymbol{y}, \boldsymbol{v})$ of the kinetic theory of gases. f represents the probability density of finding an atom with velocity $\boldsymbol{v}$ in a small neighborhood of $\boldsymbol{y}$ at time t, in Eulerian form. The OMD assumption in MD has a direct analog for the Boltzmann equation, corresponding precisely to homoenergetic solutions (Dayal & James 2010; James *et al.* 2019). To understand this connection, we consider an OMD simulation with the time-dependent translation group as above, and we examine the statistics of the MD solutions. Draw a ball B_0 of any diameter centered at the origin. Now choose integers ν_1, ν_2, ν_3 and draw a ball B_ν of the same diameter centered at $\boldsymbol{y} = (\boldsymbol{I} + t\boldsymbol{A})(\nu_1 \boldsymbol{e}_1 + \nu_2 \boldsymbol{e}_2 + \nu_3 \boldsymbol{e}_3)$. Since the simulated atoms quickly diffuse into the nonsimulated atoms during a simulation, it is not unusual that B_0 and B_ν at any particular time contain some simulated atoms and some nonsimulated atoms. The velocities of atoms in B_0 and B_ν are different. Nevertheless, if we know the velocities of atoms in B_0, then we can calculate by explicit formulas the velocities of atoms in B_ν. But, based on its interpretation, this must imply an ansatz for

† Email address for correspondence: james@umn.edu

the molecular density function f. It is

$$f(t, \boldsymbol{x}, \boldsymbol{v}) = g(t, \boldsymbol{v} - \boldsymbol{A}(\boldsymbol{I} + t\boldsymbol{A})^{-1}\boldsymbol{x}) = g(t, \boldsymbol{w}). \tag{1.2}$$

On substituting this OMD ansatz into the general form of the Boltzmann equation, we obtain an exact reduction to an equation for $g(t, \boldsymbol{w})$. Here, $\boldsymbol{w}$ is nothing but the thermal velocity where the mean velocity $(\boldsymbol{A}(\boldsymbol{I}+t\boldsymbol{A})^{-1}\boldsymbol{x})$ is subtracted from the velocity $\boldsymbol{v}$.

In the near-equilibrium limit the Chapman-Enskog (CE) expansion leads to a CE density function (DF) which reduces the conservation equations to the Navier-Stokes equations. The CE distribution function for OMD flows in terms of viscous stress tensor is written as (Boyd & Schwartzentruber 2017)

$$g(\boldsymbol{w}) = g_0(\boldsymbol{w})(1 + \Phi(\boldsymbol{w})),$$

where

$$\Phi(\boldsymbol{w}) = \frac{-m}{pk_bT}\left[\tau_{12}w_1w_2 + \tau_{13}w_1w_3 + \tau_{23}w_2w_3 + \frac{1}{2}\tau_{11}(w_1^2 - w_3^2) + \frac{1}{2}\tau_{22}(w_2^2 - w_3^2)\right]$$

$$g_0(\boldsymbol{w}) = \frac{m}{(2\pi k_bT)^{3/2}}\exp\left(\frac{-m}{2k_bT}(w_1^2 + w_2^2 + w_3^2)\right).$$

The in-plane DF is obtained by averaging over all the thermal velocities in $\boldsymbol{e}_3$ direction. This leads to

$$g(w_1, w_2) = \frac{0.0635m}{k_b^2pT^2}\exp(-\frac{m}{2k_bT}(w_1^2 + w_2^2))\Bigg(2.506k_bpT + 1.253(k_bT - mw_1^2)\tau_{11} - 2.506mw_1w_2\tau_{12} + 1.253(k_bT - mw_2^2)\tau_{22}\Bigg).$$

This CE density function further reduces for uniform simple-shear OMD flows to

$$g(w_1, w_2) = \frac{0.0635m}{k_b^2pT^2}\exp(-\frac{m}{2k_bT}(w_1^2 + w_2^2))2.506\Bigg(k_bpT - mw_1w_2\tau_{12}\Bigg),$$

where $\tau_{ii} = 0$ and $\tau_{12} = \mu_{\mathrm{NSF}}\kappa$

In Fig. 1 we plot this reduced density function g in the $w_1 - w_2$ plane at $t = 1.62$ x 10^9 s for $\kappa = 4.6$ x 10^9 s^{-1}. A large shear rate has been chosen to eliminate noise in the system and hence make the feature apparent. Dashed red and solid black lines points along in-plane eigenvectors $(\Lambda_{\sigma_2}, \Lambda_{d_2})$ corresponding to eigenvalues (σ_2 and d_2) of OMD computed stress tensor $\boldsymbol{\sigma}$ and $\boldsymbol{d}$ respectively. The maximum of the density function is achieved along $x = |y|(\theta_{d_2} = 45°, \theta_{d_2} = 135°)$ line. This indicates presence of shear stress τ_{12} in accordance with the Boltzmann definition of the stress tensor (1.3) based on thermal velocity.

$$\boldsymbol{\sigma} = \langle\frac{\rho}{N}\sum_i^N\left[\boldsymbol{v}_i' \otimes \boldsymbol{v}_i'\right]\rangle. \tag{1.3}$$

This also verifies the underlying assumption of collinearity of stress tensor $\boldsymbol{\sigma}$ and strain rate tensor $\boldsymbol{d}$ inherent in Navier-Stokes relation and hence is reflected in near-equilibrium CE analysis derived VDF.

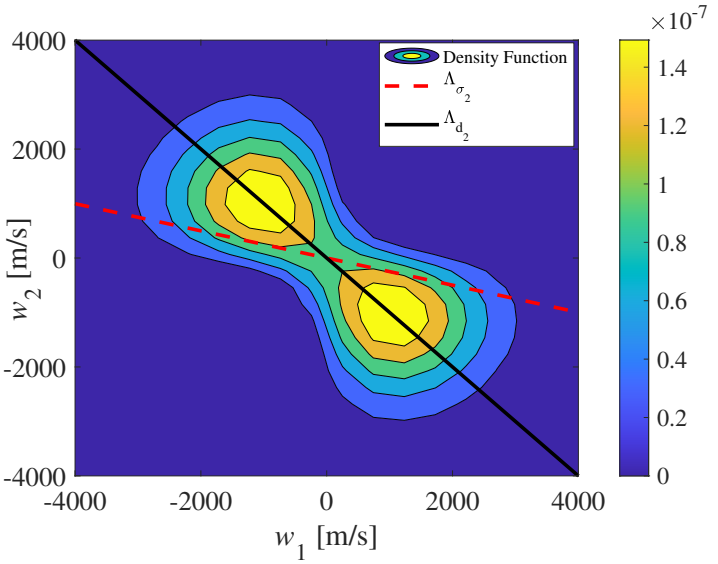

Figure 1: Snapshot of Chapman-Enskog reduced density function $g(w_1, w_2)$. Red and black solid lines points along in-plane eigenvectors corresponding to eigenvalues (σ_2 and d_2) of OMD computed stress tensor ($\boldsymbol{\sigma}$) and strain rate tensor $\boldsymbol{d}$.

Fig. 2(a) plots the distribution function computed from OMD simulation which shows the inability of CE type distribution to describe the correct statistics of atoms under highly non-equilibrium conditions. It is obtained by discretizing the $w_1 - w_2$ plane into small bins and analyzing the statistics of the simulated atoms in the fundamental domain. The OMD computed distribution is qualitatively very different than CE and also shows the existence of ellipticity which is aligned along an eigenvector of stress tensor ($\theta_{\sigma_2} \approx 165^\circ$) computed using (1.3) and hence indicates lagging in $w_1 - w_2$ plane, confirming the failure of collinearity assumption. Thus the assumption underlying Reiner-Rivlin constitutive equation that the stress tensor is, apart from hydrostatic pressure, a function of velocity gradient only is not generally valid for dilute gas under large rates. A theory which could relax this assumption will be more suitable for deriving accurate constitutive relations.

2. Comparison between OMD and Burnett's viscometric functions for Lennard Jones and hard-sphere gas under uniform simple shear respectively.

The form of the RE model for simple shear is given by

$$\tau = -\mu[\boldsymbol{A}_1 - \frac{\mathrm{tr}(\boldsymbol{A}_1)}{3}\boldsymbol{I}] - \alpha_1[\boldsymbol{A}_2 - \frac{\mathrm{tr}(\boldsymbol{A}_2)}{3}\boldsymbol{I}] - \alpha_2[\boldsymbol{A}_1^2 - \frac{\mathrm{tr}(\boldsymbol{A}_1^2)}{3}\boldsymbol{I}],$$

$$\tau_{12} = -(\kappa\mu),\ \tau_{11} = (\frac{4}{3}\kappa^2\alpha_1),\ \tau_{22} = \tau_{33} = (\frac{-2}{3}\kappa^2\alpha_1)$$

$$\mu^* = \frac{1}{1 + c_1(s^*)^{c_2}}, \quad \alpha_1^* = \frac{1}{2}(c_3 + c_4(s^*)^{c_5})^{c_6}, \quad \alpha_2 = -2\alpha_1, \tag{2.1}$$

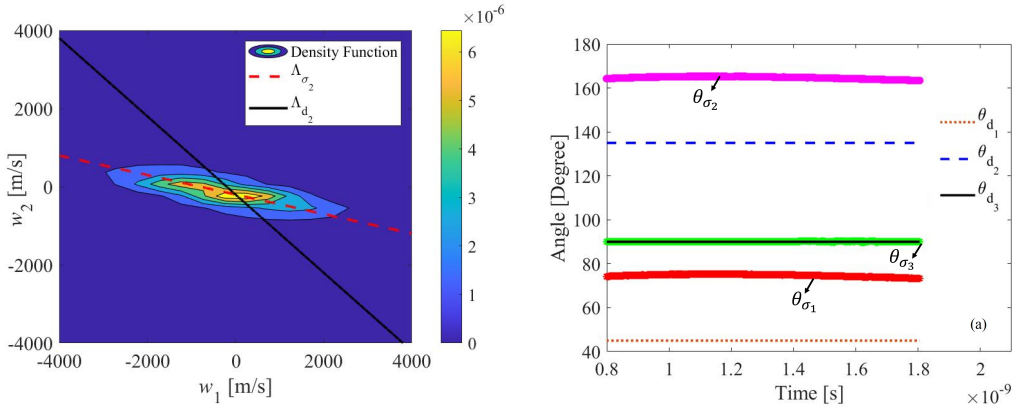

(a) (b)

Figure 2: (a) Snapshot of OMD reduced density function $g(w_1, w_2)$. Red dashed and black solid lines points along in-plane eigenvectors corresponding to eigenvalues (σ_2 and d_2) of OMD computed stress tensor ($\boldsymbol{\sigma}$) and strain rate tensor $\boldsymbol{d}$ respectively. (b) Time evolution of the angles enclosed by eigenvectors of stress tensor $\boldsymbol{\sigma}$ and $\boldsymbol{d}$ with $\boldsymbol{e}_1$.

$$\mu^* = \mu/\mu_{\text{NSF}}, \quad \alpha_1^* = p\alpha_1/\mu_{NSF}^2, \; s^*(t) = \frac{\sqrt{2}\kappa}{\nu(T(t))} = \frac{\sqrt{2}\kappa\mu_{\text{NSF}}(t)}{p(t)} \tag{2.2}$$

Two normalized normal stress differences for $\boldsymbol{v}(\boldsymbol{x}, t) = \boldsymbol{A}(\boldsymbol{I} + t\boldsymbol{A})^{-1}\boldsymbol{x} = \kappa x_2 \boldsymbol{e}_1$ reduces to:

$$N_1 = N_1(s^*(t)) = -(\tau_{11} - \tau_{22})/p = (\frac{-2}{3}\frac{\kappa^2\alpha_1}{p}) - (\frac{4}{3}\frac{\kappa^2\alpha_1}{p}) = -2\kappa^2\alpha_1 = -\frac{2\kappa^2\mu_{NSF}^2}{p^2}\alpha_1^*$$

$$N_2 = N_2(s^*(t)) = -(\tau_{22} - \tau_{33})/p = (\frac{2}{3}\frac{\kappa^2\alpha_1}{p}) - (\frac{2}{3}\frac{\kappa^2\alpha_1}{p}) = 0 \tag{2.3}$$

where α_1^* is a function of breakdown parameter s^* and is non-negative. It can be seen from (2.3) and Fig. 1 in the previous study (Pahlani *et al.* 2022) that first normal stress difference N_1 is negative and second normal stress difference identically vanishes.

The exact Burnett order equation for simple shear is given by (Comeaux *et al.* 1995)

$$\tau = \tau^1 + \tau^2 = -2\mu_{\text{NSF}}\overline{\nabla \boldsymbol{v}} + \cancel{\omega_1\frac{\mu^2}{p}\overline{\nabla\cdot\boldsymbol{v}\nabla\boldsymbol{v}}} + \omega_2\frac{\mu^2}{p}(\cancel{\frac{D}{Dt}\overline{\nabla\boldsymbol{v}}} - 2\overline{\nabla\boldsymbol{v}\nabla\boldsymbol{v}})$$
$$+\cancel{\omega_3\frac{\mu^2}{\rho T}\overline{\nabla\nabla T}} + \cancel{\omega_4\frac{\mu^2}{\rho p T}\overline{\nabla p\nabla T}} + \cancel{\omega_5\frac{\mu^2}{\rho T^2}\overline{\nabla T\nabla T}} + \omega_6\frac{\mu^2}{p}\overline{\nabla\boldsymbol{v}}\;\overline{\nabla\boldsymbol{v}}, \tag{2.4}$$

$$= -2\mu_{\text{NSF}}\begin{bmatrix}0 & \kappa & 0\\ \kappa & 0 & 0\\ 0 & 0 & 0\end{bmatrix} + (-2)\omega_2\frac{\mu^2}{p}\begin{bmatrix}-\kappa^2/6 & 0 & 0\\ 0 & \kappa^2/3 & 0\\ 0 & 0 & -\kappa^2/6\end{bmatrix} + \omega_6\frac{\mu^2}{p}\begin{bmatrix}\kappa^2/6 & 0 & 0\\ 0 & \kappa^2/6 & 0\\ 0 & 0 & -\kappa^2/3\end{bmatrix} \tag{2.5}$$

$$\tau_{12} = -2\kappa\mu_{\rm NSF},\ \tau_{11} = \frac{\kappa^2\mu_{\rm NSF}^2}{6p}(2\omega_2+\omega_6),\ \tau_{22} = \frac{\kappa^2\mu_{\rm NSF}^2}{6p}(-4\omega_2+\omega_6),\ \tau_{33} = \frac{\kappa^2\mu_{\rm NSF}^2}{6p}(2\omega_2-2\omega_6) \tag{2.6}$$

where $\omega_2 = 2,\ \omega_6 = 8$ for hard sphere gas (Comeaux *et al.* 1995) and spatial gradients of temperature and density fields are identically zero canceling some terms in (2.4). The two normalized normal stress differences for Burnett hard sphere simple shear gas reduces to

$$N_1 = N_2 = -2\frac{\kappa^2\mu_{NSF}^2}{p^2} \tag{2.7}$$

This suggests that sign of first normal stress difference predicted by the proposed RE model (Lennard-Jones gas) and Burnett model (Hard-sphere gas) are the same. However, the second normal stress difference derived from the RE model is identically zero, in contrast to the Burnett model which predicts the equivalence of N_1 and N_2. Additionally N_1 depends on the velocity gradient through α_1. Note that OMD is derived for LJ gas whereas Burnett is derived for hard sphere gas.

3. OMD solution of uniform simple shear flow of Maxwellian molecules.

The constitutive response of gas is characterized by material functions. In this section, we compute these material functions for simple shear flow of Maxwellian molecules where the interatomic force between two atoms i and j at distance r_{ij}, is given by

$$\phi(\mathbf{r}_{ij}) = 48\frac{\epsilon}{r_{ij}^2}(\frac{\sigma}{r_{ij}})^4\mathbf{r}_{ij} \tag{3.1}$$

where $\epsilon = 1.65\times10^{-21}$J, $\sigma = 3.4\times10^{-10}$m. The details on the setup of OMD is provided in Appendix A and in the previous work (Pahlani *et al.* 2023).

The definition of dimensionless material functions for uniform simple shear flow $\boldsymbol{A} = \kappa\boldsymbol{e}_1\otimes\boldsymbol{e}_2$ are given by (Garzó & Santos 2003)

$$F_\eta(\kappa^*) = -lim_{t\to\infty}\frac{\nu}{\kappa}\frac{\tau_{12}(t)}{p(t)}$$

$$\Psi_1(\kappa^*) = lim_{t\to\infty}\frac{\nu^2}{\kappa^2}\frac{\tau_{22}(t)-\tau_{11}(t)}{p(t)}$$

$$\Psi_2(\kappa^*) = lim_{t\to\infty}\frac{\nu^2}{\kappa^2}\frac{\tau_{33}(t)-\tau_{22}(t)}{p(t)}$$

where $\kappa^* = \kappa/\nu$ is reduced shear rate, κ is shear rate and ν is collision frequency of the gas. For the force field given by (3.1), the collision frequency of Maxwellian molecules is given by (Truesdell & Muncaster 1980).

$$\nu = \frac{p}{\mu} = \sqrt{\frac{48\epsilon\sigma^4}{2m^3}}3a\rho = 5.534\text{ x }10^9\rho\text{ s}^{-1}$$

where p is pressure, μ is viscosity, ϵ and σ are force field interaction parameters given in eq. (3.1), $m = 6.6335$ x 10^{-26} kg is mass of an argon atom, $a = 1.37$ for Maxwellian molecules and ρ is density of gas which is chosen to be 0.1784 kg/m^3 for the OMD

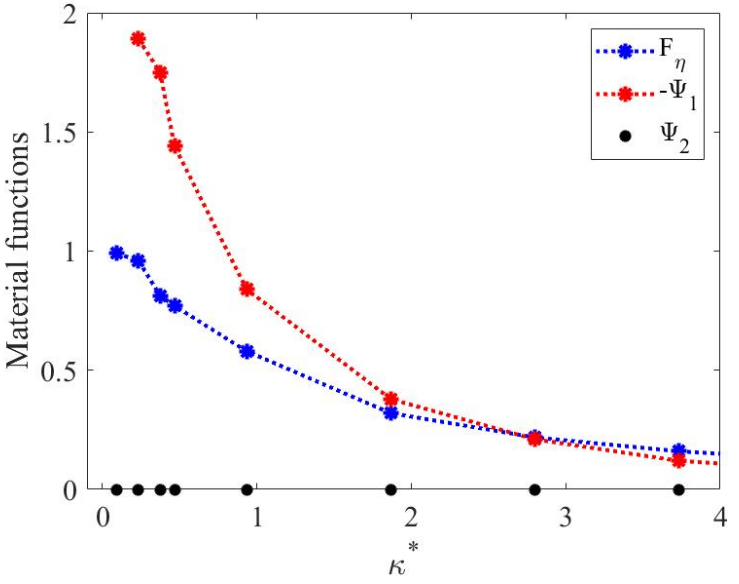

Figure 3: Material functions as function of reduced shear rate (Maxwell molecules). These results agree well with the analytical results from the kinetic theory, see (Garzó & Santos 2003)

simulation performed here. It is important to note that inverse fifth power interaction considered here leads to viscosity which varies linearly with temperature T. Due to this collision frequency remains constant as time evolves. Therefore, reduced shear rate κ^* which quantifies the departure of the system from equilibrium remains constant in time for given κ even though the temperature of the system increases with time (no thermostats). Note that this is not true for Lennard-Jones force field used in this work.

OMD evolution of the material functions are plotted in Fig. 3 against the reduced shear rate a^* given by the ratio of shear rate and collision frequency of the gas. Each data point in Fig. 3 corresponds to an independent OMD simulation (ensemble averaged over many instances of OMD simulations with varying random seeds for initial positions and velocities) with different κ. The data (in Table 1) is extracted when the system reaches a steady state at given κ^*. As κ^* decreases, the computational expense of simulation and statistical fluctuations increases.

It can be observed that the third material function Ψ_2 is identically zero which is the characteristic of Maxwellian molecules. The other two functions F_η and Ψ_1 are monotonically decreasing functions of κ^*. As κ^* increases, F_η reduces which provides evidence of the shear thinning effect. There exists a close comparison between the behavior of gas observed here in Fig. 3 and the previous work (Garzó & Santos 2003) (Chapter2, Fig. 2.3) where the continuum equations obtained by moment expansion of the Boltzmann equation was used to derive these steady-state functions analytically. In addition to providing insights into the non-equilibrium behavior of Maxwellian gas, this investigation provides the validation of the numerical approach of OMD.

κ^*	$F_\eta(\kappa^*)$	$-\Psi_1(\kappa^*)$
0.0934	0.99	-
0.2332	0.96	1.89
0.3733	0.813	1.75
0.4699	0.77	1.44
0.9332	0.581	0.84
1.867	0.32	0.379
2.800	0.218	0.21
3.734	0.16	0.12
4.667	0.124	0.08

Table 1: Reduced material functions as a function of reduced shear rate (Maxwell molecules: Inverse fifth power interaction)

REFERENCES

Boyd, Iain D & Schwartzentruber, Thomas E 2017 *Nonequilibrium gas dynamics and molecular simulation*, , vol. 42. Cambridge University Press.

Comeaux, Keith, Chapman, Dean, Ma & Cormack, Robert 1995 An analysis of the burnett equations based on the second law of thermodynamics. In *33rd Aerospace sciences meeting and exhibit*, p. 415.

Dayal, Kaushik & James, Richard D 2010 Nonequilibrium molecular dynamics for bulk materials and nanostructures. *Journal of the Mechanics and Physics of Solids* **58** (2), 145–163.

Garzó, Vicente & Santos, Andrés 2003 *Kinetic theory of gases in shear flows: nonlinear transport*, , vol. 131. Springer Science & Business Media.

James, Richard D, Nota, Alessia & Velázquez, Juan JL 2019 Self-similar profiles for homoenergetic solutions of the boltzmann equation: particle velocity distribution and entropy. *Archive for Rational Mechanics and Analysis* **231** (2), 787–843.

Pahlani, Gunjan, Schwartzentruber, Thomas E & James, Richard 2022 Investigation of the breakdown of navier-stokes equation using objective molecular dynamics. In *AIAA SCITECH 2022 Forum*, p. 1012.

Pahlani, Gunjan, Schwartzentruber, Thomas E & James, Richard D 2023 Objective molecular dynamics for atomistic simulation of macroscopic fluid motion. *Journal of Computational Physics* p. 111938.

Reiner, Markus 1945 A mathematical theory of dilatancy. *American Journal of Mathematics* **67** (3), 350–362.

Rivlin, RS 1997 Forty years of non-linear continuum mechanics. In *Collected Papers of RS Rivlin*, pp. 2783–2811. Springer.

Truesdell, Clifford & Muncaster, Robert G 1980 *Fundamentals of Maxwel's Kinetic Theory of a Simple Monatomic Gas: Treated as a Branch of Rational Mechanics*. Academic Press.